

Cite this: *Digital Discovery*, 2024, 3, 602

# Infrared spectra prediction using attention-based graph neural networks†

Naseem Saquer,<sup>ID</sup> <sup>a</sup> Razib Iqbal,<sup>ID</sup> <sup>\*b</sup> Joshua D. Ellis<sup>b</sup> and Keiichi Yoshimatsu <sup>ID</sup> <sup>\*a</sup>

Infrared (IR) spectroscopy is an analytical technique that is used in broad disciplines of fundamental and applied research areas. Along those lines, it is of significant interest to develop an efficient computational method for the prediction of IR spectra based on chemical structures. In this work, we investigated the performance of attention-based graph neural networks. Our study showed that AttentiveFP model, which incorporates the message passing and graph attention mechanisms, exhibits the highest performance among the tested graph neural network models and a benchmark descriptor-based model. The implication is that the capability of AttentiveFP model to learn interactions between neighboring atoms and distant atoms allows for improving the performance of IR spectra prediction model. The mean Spearman correlation coefficient between the IR spectra predicted by AttentiveFP model and actual spectra was 0.911 and the correlation coefficient values were above 0.8 in 88% of the test cases. Our findings demonstrate the utility of the graph attention mechanism for the development of graph neural network-based machine learning models for IR spectra prediction with improved performances.

Received 23rd December 2023

Accepted 17th January 2024

DOI: 10.1039/d3dd00254c

rsc.li/digitaldiscovery

## 1 Introduction

Infrared (IR) spectroscopy is an analytical technique that is used in broad areas including chemical,<sup>1,2</sup> materials,<sup>3</sup> biological,<sup>4–7</sup> environmental,<sup>8</sup> and astrophysical<sup>9,10</sup> sciences. Since the absorption of IR radiation provides information on the vibrations of the chemical bonds, IR spectroscopy is widely used for the structural analysis and/or identification of compounds. While there are a number of established computational approaches including the vibrational calculations with the harmonic approximation for IR spectra prediction, the accuracy of these approaches depend on the quality of the theoretical description of many factors including anharmonic effects.<sup>11</sup> Therefore, the accurate prediction of IR spectra by such methods requires a substantial computational cost and has some limitations. Along those lines, it is of significant interest to develop a new approach for the accurate prediction of IR spectra with a lower computational cost.

The application of machine learning (ML) in molecular property prediction is rapidly gaining momentum.<sup>12–15</sup> To date, there have been many reports on successful applications of ML

methods in broad areas including the prediction of drug-like properties, water solubility, protein–ligand affinity, toxicity, and quantum mechanical properties based on molecular structures.<sup>12–15</sup> In terms of IR spectra prediction, Gastegger *et al.* have used ML models to circumvent electronic structure calculations and account for vibrational anharmonic and dynamical effects in *ab initio* molecular dynamics (AIMD)<sup>16</sup> as well as solvent effects.<sup>17</sup> In other works, the n2p2 ML package has been applied in IR spectra prediction for the calculation of electronic structures and molecular dipoles along with the GVPT2 method for anharmonic corrections.<sup>18,19</sup> Meanwhile, these approaches use ML methods to accelerate one or more of computationally expensive steps in electronic structure calculations. An alternative approach is to develop ML models that directly map IR spectra from chemical structures without electronic structure calculations.<sup>20–23</sup> ML models of this type were first reported by Affolter and Clerc<sup>20</sup> and subsequently by Weigel and Herges<sup>21</sup> in 1990s. The reported models consist of dense neural networks (DNN) that take engineered structure descriptors<sup>24</sup> as inputs. While the capabilities of these models were limited in terms of the resolutions of spectral data, the amount of training data being employed, simpler data representations, and smaller network sizes due to the limited computational powers available at that time, these early works showed the promise of ML methods in IR spectra prediction. Recently, Kovács *et al.*<sup>22</sup> have reported the application of ML models that pass the Morgan fingerprints (MorganFP)<sup>25</sup> of compounds into larger DNNs for IR spectra prediction of polyaromatic hydrocarbons at a high resolution. Meanwhile, these ‘direct IR spectra mapping’ ML models<sup>20–22</sup> used various molecular

<sup>a</sup>Department of Chemistry and Biochemistry, Missouri State University, 901 South National Avenue, Springfield, MO 65897, USA. E-mail: KYoshimatsu@MissouriState.edu; Tel: +1 417 836 5613

<sup>b</sup>Department of Computer Science, Missouri State University, 901 South National Avenue, Springfield, MO 65897, USA. E-mail: RIqbal@MissouriState.edu; Tel: +1 417 836 4944

† Electronic supplementary information (ESI) available: Supporting tables and figures on the composition of dataset, histogram of correlation coefficient values for all tested models, and attention values. See DOI: <https://doi.org/10.1039/d3dd00254c>



descriptors including MorganFP and other “hand-engineered” molecular descriptors<sup>26</sup> as the structural representations of compounds. It has been known that the performance of ML models often depends on the data representation and architecture of the models.<sup>27</sup>

Over the last several years, graph neural network-based ML models, which are capable of directly operating on molecular graphs,<sup>24,28–30</sup> are attracting a great deal of attention for their advantages in eliminating the step for engineering task-specific descriptors. McGill *et al.* have recently reported that message passing neural network (MPNN) models, a type of graph neural network model with the message passing mechanism, outperformed a descriptor-based model that uses MorganFP on IR spectral prediction.<sup>23</sup> However, to our best knowledge, graph neural networks other than MPNN have not been applied in IR spectra prediction. We therefore set out to investigate the performance of other graph neural network-based models in IR spectra prediction. Herein, we report the application of graph neural network models that incorporate the graph attention mechanism<sup>31</sup> in direct mapping of IR spectra from chemical structures. We trained and evaluated the performance of a descriptor-based model (MorganFP/DNN) and four graph neural network models that are built upon different architectures including AttentiveFP, which has been reported to show high performances in several chemical property prediction tasks<sup>30,32</sup> by incorporating the graph attention mechanism in conjunction with the message passing mechanism, along with graph convolutional neural network (GCN), graph attention network (GAT), and MPNN. Our results indicate that the graph attention mechanism can be used as an effective method to improve the performance of graph neural networks in complex chemical property prediction tasks.

## 2 Methods

### 2.1 Dataset

IR spectra and structures of 16 000 compounds were retrieved from the NIST Chemistry WebBook (Evaluated Infrared Reference Spectra in NIST Standard Reference Database Number 69)<sup>33</sup> using a modified BeautifulSoup script.<sup>34</sup> The data were stored as MOL files describing the chemical structure and JDX files recording numerical spectral data and metadata for every spectrum. The largest subset of the available data comprised of the IR spectra measured in the gas phase. We therefore employed this subset of data in this study. Additionally, the compounds that do not contain at least one C–H bond (96 compounds), ones containing formal charges (640 compounds), and ones containing more than 25 non-hydrogen atoms (120 compounds) were excluded from the dataset. The final dataset used in this work consisted of 7505 samples.

The dataset consists of diverse classes of compounds (Tables 1 and 2). As shown in Table 1, approximately 55% of the compounds in the dataset contain at least one aromatic ring. Out of the rest, 33% are acyclic compounds and 22% are non-aromatic, cyclic compounds. In terms of atomic compositions, the majority (63%) of the compounds are comprised of only C, H, O, and/or N atoms and 36% contained halogens, sulfur, and/

Table 1 Composition of dataset by the carbon backbone structures

Type	Count
Acyclic	2493
Cyclic (non-aromatic)	885
Cyclic (aromatic)	4127

Table 2 Composition of dataset by atoms

Atoms contained	Count
CH only	868
CHO only	2424
CHN only	566
CHON only	839
Contains halogens, sulfur, and/or phosphorus	2728
Others <sup>a</sup>	80
Total	7505

<sup>a</sup> Compounds containing B, Si, Se, Sn, and/or Hg.

or phosphorous atoms (Table 2). A small number of compounds in the dataset contained other atoms including B, Si, Se, Sn and/or Hg. We also confirmed that compounds containing a broad range of functional groups are present within the dataset (Table S1 in ESI†). The compounds in the dataset consist of 11.39 non-hydrogen atoms in average (Fig. S1 in ESI†).

### 2.2 Preprocessing of spectra

During data preprocessing, all IR spectra were normalized and converted to a series of 1800 data points covering the wavenumber range of 450 cm<sup>-1</sup> to 4050 cm<sup>-1</sup> with an increment of 2 cm<sup>-1</sup>. An example of preprocessed IR spectra is shown in Fig. 1. All units in the x-axis and y-axis were converted to wavenumbers and absorbance values, respectively. The absorbance values on each spectrum were linearly normalized to range from 0 to 1 using the following equation:

$$\text{Abs}(\text{norm}, x) = \frac{\text{Abs}(x)}{\text{Abs}(\text{max})} \quad (1)$$

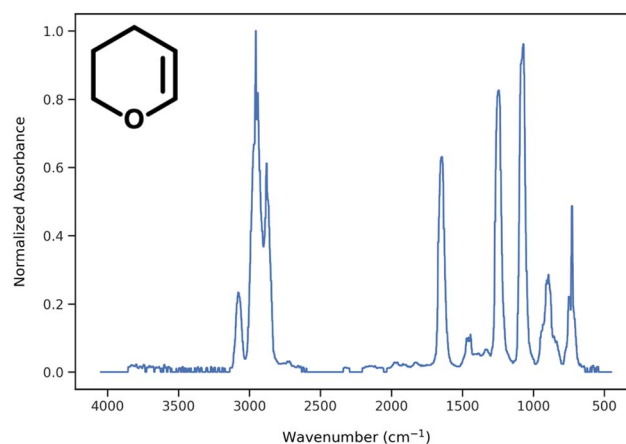


Fig. 1 Example of normalized IR spectrum after preprocessing.



where Abs(max) is the highest absorbance value observed in the spectrum and Abs( $x$ ) is the absorbance at wavenumber  $x$ .

### 2.3 Neural network models

All untrained neural network models (GCN, GAT, MPNN, AttentiveFP, DNN) were imported from the DeepChem library<sup>35</sup> and trained as described below. Each model takes the structural data saved as molecular graph objects or MorganFP descriptors and the preprocessed spectral data as inputs. The RDKit library<sup>36</sup> was used to convert the structural data into SMILES and then to MorganFP. The DeepChem library<sup>35</sup> was used to convert the SMILES into molecular graph objects.

**2.3.1 Graph convolutional network (GCN).** We chose GCN as a baseline graph neural network model, which converts a molecular graph of any size into a fixed length vector by aggregating each node's features into a single vector representing the whole molecule.<sup>29</sup> This model was implemented with 64 output channels across two graph convolution (Graph-Conv) layers, and one intermediate dense layer connecting to the output layer. Sigmoid activations were used for each of these layers.

**2.3.2 Graph attention network (GAT).** GAT is a variant of GCNs with the attention mechanism, which aims to mimic cognitive attention by emphasizing certain parts of the input data.<sup>31</sup> The self-attention layers specify weights to different nodes during node aggregation steps. This allows for the network to learn the most important local features within structures during the training process. Two graph attention (GAT) layers with 64 output channels were used in this work. These layers were connected to three consecutive dense layers of 2048 neurons with ReLU activation functions.

**2.3.3 Message passing neural network (MPNN).** MPNN is another type of graph convolutional network architecture which transmits information of each node to all nodes with an entire molecular graph by a so called message passing process. In MPNNs, the feature vectors in each node are iteratively updated by aggregating feature vectors of neighboring nodes.<sup>37</sup> Therefore, each node that underwent message passing incorporates information about the overall molecule. In this work, features were aggregated by taking the mean of each neighboring node's feature vectors. A single graph layer performed 5 iterations of message passing and the graph layer is connected with subsequent two dense layers of 2048 neurons with ReLU activation functions.

**2.3.4 AttentiveFP.** AttentiveFP network architecture utilizes both the message passing and graph attention mechanisms in graph convolution.<sup>30</sup> In each iteration during training, an AttentiveFP network aggregates feature vectors of neighboring nodes and updates attention values in order to 'learn' the properties of each atom by accounting for the influences of both nearby and distant atoms. Two iterations of message passing occurred for each molecule in each of the two graph layers that are connected to a dense layer of 2048 neurons. Each layer had a ReLU activation function applied.

**2.3.5 MorganFP/DNN.** Morgan fingerprint (MorganFP) is one of the most widely used descriptors for representing

chemical structures to train ML models in cheminformatics.<sup>25</sup> In this work, a dense neural network (DNN) that takes extended-connectivity fingerprints with a radius of 2 and length of 1024 bits as an input was trained and evaluated as a benchmark network model. The fingerprint went through dense layers with 4096, 2048, and 1024 neurons which all had ReLU functions applied to them. The output layer had a sigmoid activation applied to it.

### 2.4 Training

Each model was trained using a batch size of 64 substances for 100 epochs. The hyperparameters were optimized using Gaussian process hyperparameter optimization. In order to fully leverage the limited amount of data on hand, 5-fold cross validation was used. In case there are multiple spectra for a single compound, all entries for the same compound are placed into the same fold. For each iteration of training and testing, 4 folds were used to train a model and 1 fold was used to test the performance. Euclidean distances between the predicted and actual spectra of each compound were used as the loss function for the training of each model.

### 2.5 Evaluation of prediction performance

For evaluation, predicted and actual spectra were smoothed over by applying a Gaussian Convolution function with a standard deviation of  $6\text{ cm}^{-1}$  using the SciPy library<sup>38</sup> in order to remove noise in low absorbance regions in the spectra. The mean of Spearman and Pearson correlation coefficients between predicted and actual spectra were then calculated and used as the metric to evaluate the performance of the trained models.

### 2.6 Comparison of different models

To compare the behavior of the trained models, we calculated Spearman and Pearson correlation coefficients between spectra that were generated by different models for each respective compound. The average values of these correlation coefficients were used to gain insights on the similarity between each pair of models.

## 3 Results and discussion

### 3.1 Performance of ML models

Table 3 summarizes the performance of each model based on Spearman and Pearson correlation coefficients between predicted and actual spectra. GCN, the baseline graph convolutional network model, and GAT, a variant of GCN with the attention mechanism, showed reasonably good yet the lowest performances. It should be noted that these two models showed lower performances in comparison to MorganFP/DNN, the benchmark molecular descriptor-based model. On the other hand, MPNN and AttentiveFP, which utilize the message passing mechanism, showed superior performances in comparison to GCN and GAT. This result indicates that the propagation of node information to neighboring atoms through the message passing mechanism led to an improved



**Table 3** Comparison of IR spectra prediction performance of five ML models based Spearman correlation coefficients between actual and predicted IR spectra. The presented values are the average of five mean Spearman correlation coefficient values from 5-fold cross validation

Model name	Spearman	Pearson
MorganFP/DNN	0.899	0.863
GCN	0.847	0.855
GAT	0.851	0.855
MPNN	0.890	0.910
AttentiveFP	0.911	0.925

performance. Among all tested models, AttentiveFP showed the best performance with the mean Spearman and Pearson correlation coefficient values of 0.911 and 0.925, respectively. As shown in Fig. 2, a closer look of the data indicated that AttentiveFP outperforms MPNN and MorganFP/DNN when we compare the values at each displayed percentile (10th, 25th, 50th, 75th, and 90th) of Spearman correlation coefficients. In particular, the 10th percentile value for AttentiveFP was higher by 4.0% and 10.6% over MPNN and MorganFP/DNN, respectively. This implies that the application of the graph attention mechanism along with the message passing mechanism allows for the network to generate fewer poor predictions while improving the prediction accuracy for most spectra. We attributed this to the advantage of AttentiveFP that is capable of effectively learning some of the important interactions between distant atoms.

To compare the similarity of the different models, we calculated the mean Spearman correlation coefficients between the IR spectra predicted by each pair of models (Fig. 3). As it can be seen, the IR spectra predicted by GAT shared the highest similarity with GCN whereas they were less similar to MPNN and AttentiveFP. On the other hand, the spectra predicted by MPNN and AttentiveFP are similar to each other. This implies that the propagation of node information by the message

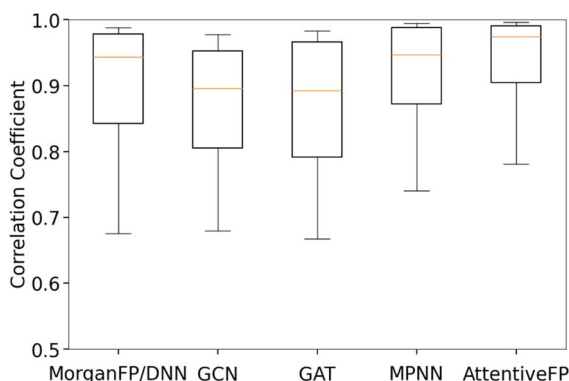


**Fig. 2** Box and whisker plot of Spearman correlation coefficients between actual and predicted IR spectra for trained models. The top and bottom borders of the boxes correspond to the 75th and 25th percentiles, respectively. The line in the middle of each box corresponds to 50th percentile. The top and bottom whiskers correspond to the 90th and 10th percentiles, respectively.

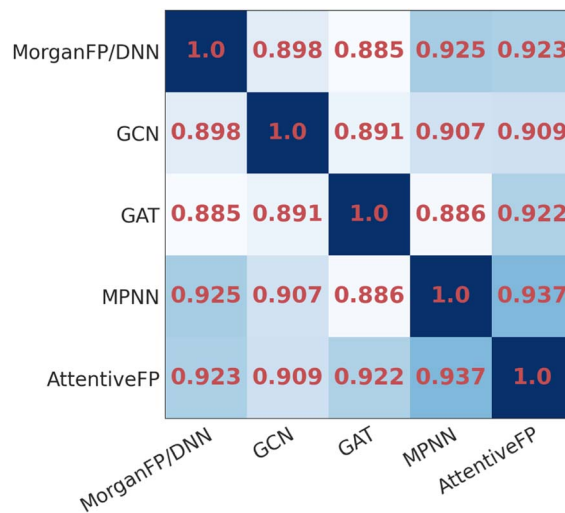


**Fig. 3** The heatmap of the mean Spearman correlation coefficients of the spectra predicted by different model pairs for identical compounds.

passing mechanism substantially affects the behavior of the models. It was also found that the MorganFP/DNN behaves more similarly to MPNN and AttentiveFP than GCN and GAT. A plausible interpretation for this is that MorganFP/DNN is capable of learning interactions between both neighboring and distant atoms as long as they are within the predetermined radius, making the model more similar to MPNN and AttentiveFP.

Fig. 4 shows the distribution of correlation coefficient values between actual spectra and spectra predicted by AttentiveFP model, which showed the highest performance. The correlation coefficients of the predicted and actual spectra are 0.9 or higher in approximately 76% of the predicted spectra. As it can be seen, these predicted spectra exhibited high similarity to their corresponding actual spectra. Approximately 12% of the predicted spectra showed moderately high correlation coefficients, 0.80–0.90. In those cases, the location of peaks are often correctly predicted while there appeared to be a tendency of the relative peak intensities being less accurately predicted. Approximately 12% of the predicted spectra had correlation coefficients below 0.8. However, it is worth noting that these comparatively less accurate spectra still often contain some of the major features of actual spectra. In a limited number of cases, as can be seen in the spectrum shown on the bottom right of Fig. 4, the predicted spectra contain large additional peaks or miss major peaks. We carried out several attempts of exploratory data analyses in order to determine if there are any trends among these poorly predicted cases. However, no clear patterns could be observed.

### 3.2 Factors that affect the IR spectra prediction performance of AttentiveFP model

Fig. 5a shows the histogram of correlation coefficients between actual IR spectra and the spectra predicted by AttentiveFP model in three different spectral regions. The characteristic peaks that appear in each of these regions are: O–H, N–H, and



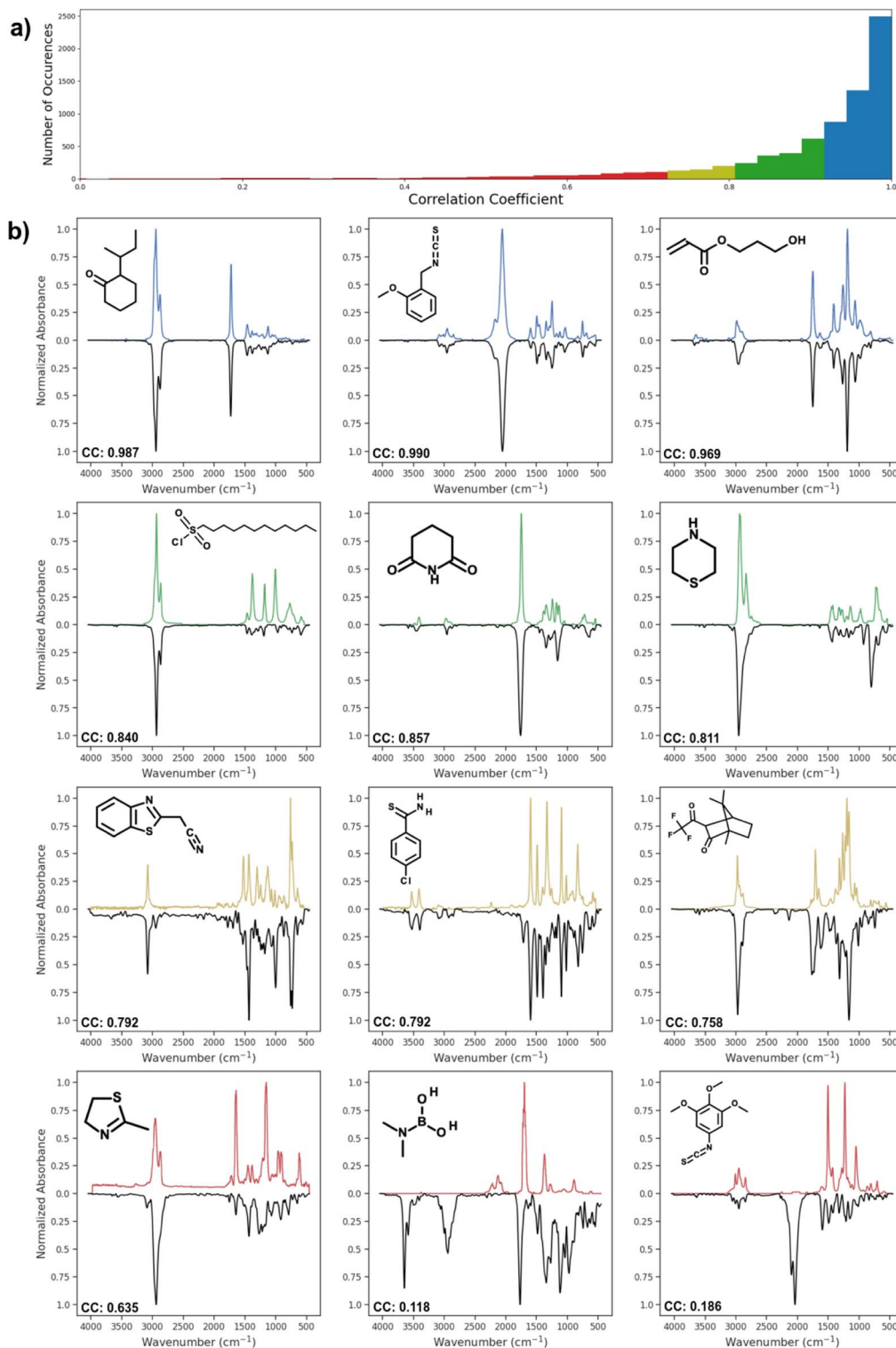


Fig. 4 (a) Distribution of Spearman correlation coefficient values between actual spectra and spectra predicted by the AttentiveFP model. (b) Predicted IR spectra by AttentiveFP model (blue, green, dark yellow, red) and actual IR spectra of the corresponding compounds (black).

C–H stretching ( $2400\text{--}4000\text{ cm}^{-1}$ ), C=O, C=N, and C=C stretching, and N–H bending ( $1500$  and  $2400\text{ cm}^{-1}$ ). As shown in Fig. 5b, the average Spearman correlation coefficient was highest in the  $2400\text{--}4050\text{ cm}^{-1}$  region followed by  $1500\text{--}2400\text{ cm}^{-1}$  region. In all three regions, the peak of each

histogram was observed in either the highest bin (above  $0.96$ ) or the second highest bin ( $0.93\text{--}0.96$ ). The 50th percentile values of the correlation coefficients are  $0.929$ ,  $0.977$ , and  $0.909$ , for the  $450\text{--}1500$ ,  $1500\text{--}2400$  and  $2400\text{--}4050\text{ cm}^{-1}$  ranges, respectively. This indicates that the model was capable of predicting the



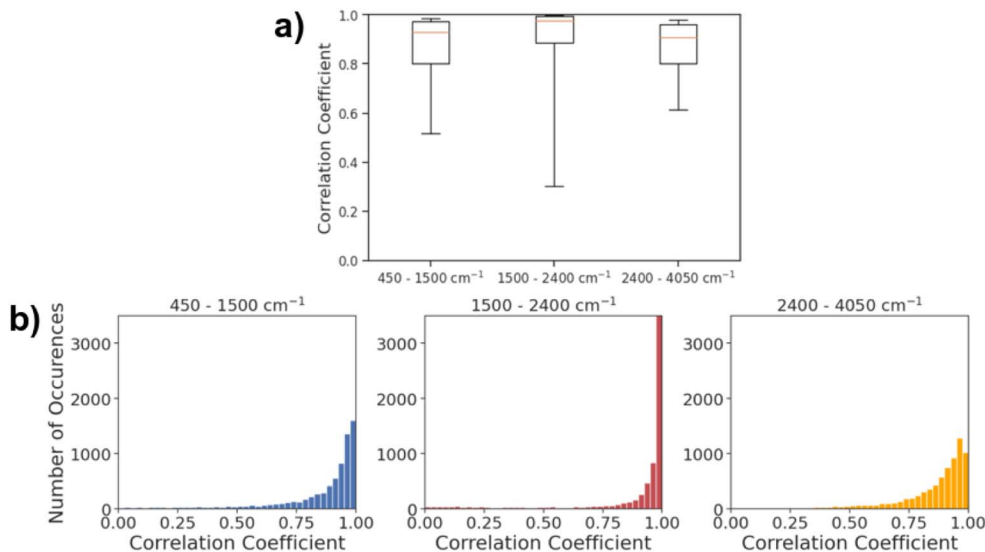


Fig. 5 (a) Box and whisker plot of Spearman correlation coefficients in various spectral regions. The top and bottom borders of the boxes correspond to the 75th and 25th percentiles, respectively. The line in the middle of each box corresponds to 50th percentile. The top and bottom whiskers correspond to the 90th and 10th percentiles, respectively. (b) Spearman correlation coefficients of predicted spectra from the AttentiveFP model and experimental data at three different spectral ranges.

spectra across the entire mid-IR range in majority of the cases. On the other hand, the 10th percentile value of the correlation coefficient for the 1500–2400 cm<sup>-1</sup> region was 0.300. This value is substantially lower than 0.519 and 0.614, respectively, for 450–1500 and 2400–4050 cm<sup>-1</sup> regions. This is reflected in Fig. 5b, as the gap between 25th percentile and 10th percentile is substantially larger in the 1500–2400 cm<sup>-1</sup> region when compared to the 450–1500 and 2400–4050 cm<sup>-1</sup> regions. The result indicates that the model predicts the spectra within 1500–2400 cm<sup>-1</sup> regions with high accuracy in more than 75% of the cases while there are a relatively small number of cases where the predicted spectra poorly resemble actual spectra. In terms of the mean Spearman correlation coefficient values, the performance of the model was comparatively lower in the 450–1500 cm<sup>-1</sup> region than other spectral regions. This is unsurprising since this spectral region is called the ‘fingerprint’ region where it is known to be highly complex due to the presence of many bands that frequently overlap with each other. This is also in line with results from past attempts at spectral prediction using machine learning, where the fingerprint region typically has the worst results.<sup>21</sup>

Finally, we investigated whether the performance of AttentiveFP model would be affected by the number of non-hydrogen atoms that are present in the compounds (Fig. 6). Interestingly, the result indicated that the performances of AttentiveFP model are not affected by the number of non-hydrogen atoms for the compounds consisting of 5 to 24 non-hydrogen atoms. Meanwhile, the comparatively lower prediction performance for the compounds consisting of 2–4 non-hydrogen atoms. Although the reasons are unclear, possible causes for this could be due to the low occurrences of these classes of molecules within the dataset (Fig. S1 in ESI<sup>†</sup>) and a higher frequency of halogenated compounds.

### 3.3 Interpretation of attention weights

At its core, attention allows neural networks to dynamically prioritize specific segments of the input data when generating output, mimicking human cognitive processes of selective concentration. Traditional sequence-to-sequence models encode inputs into fixed-size vectors, but attention facilitates a more adaptive approach. In the AttentiveFP model, an attention vector is calculated by assessing the relevance for each input–output pair, applying a softmax function, and creating a context vector from a weighted sum in order to emphasize the effects of certain molecular features that have a greater impact on the spectrum.<sup>30</sup>

We therefore looked into the attention values being assigned by the AttentiveFP model (Table S3<sup>†</sup>). In this respect we first

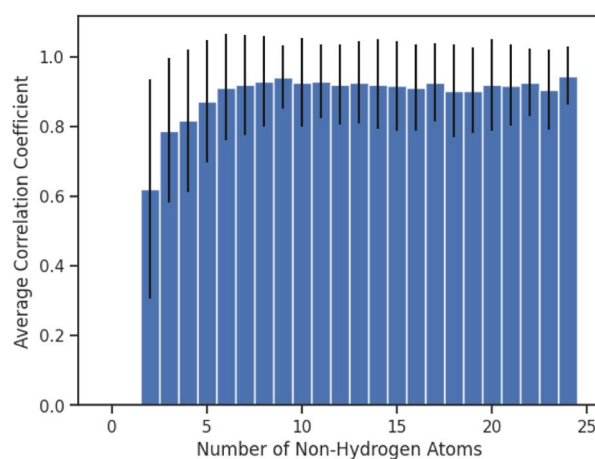


Fig. 6 Average of Spearman correlation coefficient values for compounds consisting of different numbers of non-hydrogen atoms. Error bars correspond to the standard deviation.



compared the average attention values on the atoms within pairs of structurally similar functional groups. The average attention values on the two non-hydrogen atoms in alcohols (O and adjacent C) weigh above the baseline attention values. On the other hand, atoms in thiols and alkyl halides show comparatively lower attention values which are closer to the baseline. The average attention values on the atoms on carboxylic acids are higher than the atoms on acyl halides. In the case of the AttentiveFP model reported by Xiong *et al.*<sup>30</sup> higher attention values were assigned on the atoms in aromatic systems when the model was trained to predict the number of aromatic atoms. The comparison of attention values on different classes of carbon atoms provided insights on how the attention mechanism could capture the influences of distant atoms. In contrast, our IR-spectra prediction models showed a tendency to assign higher attention values to non-aromatic carbons in alkyl chains and alkene over carbons in aromatic systems. Considering the fact that all carbon–hydrogen bonds and carbon–carbon bonds manifest different peaks on IR spectra, the observed deviations among different classes of carbon atoms are reasonable. We also confirmed that the attention values are not biased toward the more abundant functional groups (Fig. S4†). These observations collectively support that the attention mechanism allowed for the AttentiveFP model to learn the impact of adjacent and distant atoms for the IR spectra prediction task.

## 4 Conclusions

In this work, we have studied the performance of graph neural networks for the prediction of the IR spectra. Our results showed that AttentiveFP model outperformed other graph neural network models as well as MorganFP/DNN model, the benchmark descriptor-based model. Approximately 88% of the spectra generated by AttentiveFP model showed high similarity, with the correlation coefficients being 0.80 or above, to experimentally determined spectra. An interesting observation was that the average correlation coefficient values between the spectra predicted by AttentiveFP model and actual spectra for molecules consisting of 12 or more non-hydrogen atoms are similar to comparatively smaller molecules consisting of 5–11 non-hydrogen atoms. In summary, our results demonstrate that the implementation of the attention mechanism is an effective approach to improve the performance of graph neural networks in mapping IR spectra from chemical structures.

## Code availability

The codes for this paper are available at GitHub at <https://github.com/nj-saquer/IR-Spectra-Prediction-Graph-Models/>.

## Data availability

This study was carried out using publicly available data on IR spectra from the NIST Chemistry WebBook database at <https://doi.org/10.18434/T4D303>. The codes that were used to retrieve

and preprocess the datasets are available at GitHub along with other code.

## Author contributions

N. S. conceptualization, data curation, formal analysis, investigation, methodology, validation, software, visualization, writing – original draft, writing – review & editing; R. I. conceptualization, methodology, funding acquisition, investigation, project administration, supervision, writing – review & editing; J. D. E. conceptualization, data curation, methodology; K. Y. conceptualization, methodology, funding acquisition, investigation, project administration, supervision, writing – original draft, writing – review & editing.

## Conflicts of interest

There are no conflicts to declare.

## Acknowledgements

This work was supported by the NASA-Missouri Space Grant Consortium (NASA-MOSGC). N. S. was partly supported by the NASA-MOSGC undergraduate research internship program. We also acknowledge NIST for making the IR spectra data available.

## Notes and references

- 1 C. Berthomieu and R. Hienerwadel, *Photosynth. Res.*, 2009, **101**, 157–170.
- 2 J. Haas and B. Mizaikoff, *Annu. Rev. Anal. Chem.*, 2016, **9**, 45–68.
- 3 T. Theophanides, *Infrared Spectroscopy: Materials Science, Engineering and Technology*, IntechOpen, London, 2012.
- 4 M. R. Jung, F. D. Horgen, S. V. Orski, V. Rodriguez C, K. L. Beers, G. H. Balazs, T. T. Jones, T. M. Work, K. C. Brignac, S.-J. Royer, *et al.*, *Mar. Pollut. Bull.*, 2018, **127**, 704–716.
- 5 M. J. Baker, J. Trevisan, P. Bassan, R. Bhargava, H. J. Butler, K. M. Dorling, P. R. Fielden, S. W. Fogarty, N. J. Fullwood, K. A. Heys, *et al.*, *Nat. Protoc.*, 2014, **9**, 1771–1791.
- 6 K. B. Beć, J. Grabska and C. W. Huck, *Anal. Chim. Acta*, 2020, **1133**, 150–177.
- 7 T. P. Wrobel and R. Bhargava, *Anal. Chem.*, 2017, **90**, 1444–1463.
- 8 K. D. Shepherd and M. G. Walsh, *J. Near Infrared Spectrosc.*, 2007, **15**, 1–19.
- 9 G. Tinetti, T. Encrenaz and A. Coustenis, *Astron. Astrophys. Rev.*, 2013, **21**, 1–65.
- 10 G. H. Rieke, *Exp. Astron.*, 2009, **25**, 125–141.
- 11 M. Thomas, M. Brehm, R. Fligg, P. Vöhringer and B. Kirchner, *Phys. Chem. Chem. Phys.*, 2013, **15**, 6608.
- 12 J. Vamathevan, D. Clark, P. Czodrowski, I. Dunham, E. Ferran, G. Lee, B. Li, A. Madabhushi, P. Shah, M. Spitzer, *et al.*, *Nat. Rev. Drug Discovery*, 2019, **18**, 463–477.
- 13 A. C. Mater and M. L. Coote, *J. Chem. Inf. Model.*, 2019, **59**, 2545–2559.



- 14 D. C. Elton, Z. Boukouvalas, M. D. Fuge and P. W. Chung, *Mol. Syst. Des. Eng.*, 2019, **4**, 828–849.
- 15 X. Yang, Y. Wang, R. Byrne, G. Schneider and S. Yang, *Chem. Rev.*, 2019, **119**, 10520–10594.
- 16 M. Gastegger, J. Behler and P. Marquetand, *Chem. Sci.*, 2017, **8**, 6924–6935.
- 17 M. Gastegger, K. T. Schütt and K.-R. Müller, *Chem. Sci.*, 2021, **12**, 11473–11483.
- 18 J. Lam, S. Abdul-Al and A.-R. Allouche, *J. Chem. Theory Comput.*, 2020, **16**, 1681–1689.
- 19 G. Laurens, M. Rabary, J. Lam, D. Peláez and A.-R. Allouche, *Theor. Chem. Acc.*, 2021, **140**, 66.
- 20 C. Affolter and J. Clerc, *Chemom. Intell. Lab. Syst.*, 1993, **21**, 151–157.
- 21 U. Weigel and R. Herges, *Anal. Chim. Acta*, 1996, **331**, 63–74.
- 22 P. Kovács, X. Zhu, J. Carrete, G. K. Madsen and Z. Wang, *Astrophys. J.*, 2020, **902**, 100.
- 23 C. McGill, M. Forsuelo, Y. Guan and W. H. Green, *J. Chem. Inf. Model.*, 2021, **61**, 2594–2609.
- 24 O. Wieder, S. Kohlbacher, M. Kuenemann, A. Garon, P. Ducrot, T. Seidel and T. Langer, *Drug Discovery Today: Technol.*, 2020, **37**, 1–12.
- 25 D. Rogers and M. Hahn, *J. Chem. Inf. Model.*, 2010, **50**, 742–754.
- 26 R. Todeschini and V. Consonni, *Molecular Descriptors for Chemoinformatics*, Wiley, Weinheim, 2009.
- 27 C. Merkwirth and T. Lengauer, *J. Chem. Inf. Model.*, 2005, **45**, 1159–1168.
- 28 D. K. Duvenaud, D. Maclaurin, J. Iparraguirre, R. Bombarell, T. Hirzel, A. Aspuru-Guzik and R. P. Adams, *Advances in Neural Information Processing Systems 28 (NIPS 2015)*, 2015.
- 29 S. Kearnes, K. McCloskey, M. Berndl, V. Pande and P. Riley, *J. Comput.-Aided Mol. Des.*, 2016, **30**, 595–608.
- 30 Z. Xiong, D. Wang, X. Liu, F. Zhong, X. Wan, X. Li, Z. Li, X. Luo, K. Chen, H. Jiang, *et al.*, *J. Med. Chem.*, 2019, **63**, 8749–8760.
- 31 P. Veličković, G. Cucurull, A. Casanova, A. Romero, P. Liò and Y. Bengio, *Graph Attention Networks*, 2017, <https://arxiv.org/abs/1710.10903>.
- 32 D. Jiang, Z. Wu, C.-Y. Hsieh, G. Chen, B. Liao, Z. Wang, C. Shen, D. Cao, J. Wu and T. Hou, *J. Cheminf.*, 2021, **13**, 1–23.
- 33 Coblenz Society Inc., Evaluated Infrared Reference Spectra, in *NIST Chemistry WebBook*, NIST Standard Reference Database Number 69, ed. P. J. Lindstrom and W. G. Mallard, National Institute of Standards and Testing, Gaithersburg MD, accessed January, 2022, DOI: [10.18434/T4D303](https://doi.org/10.18434/T4D303).
- 34 M. Swaine, *nist.py*, 2015, <https://gist.github.com/mcs07/48f4c0f072e5f45dcaa>, accessed January, 2022.
- 35 B. Ramsundar, P. Eastman, P. Walters and V. Pande, *Deep learning for the life sciences: applying deep learning to genomics, microscopy, drug discovery, and more*, O'Reilly, Sebastopol, 2019.
- 36 G. Landrum, *RDKit: open-source cheminformatics software*, <https://rdkit.org/>.
- 37 J. Gilmer, S. S. Schoenholz, P. F. Riley, O. Vinyals and G. E. Dahl, *Proceedings of the 34th International Conference on Machine Learning, PMLR 70*, 2017, pp. 1263–1272.
- 38 P. Virtanen, R. Gommers, T. E. Oliphant, M. Haberland, T. Reddy, D. Cournapeau, E. Burovski, P. Peterson, W. Weckesser, J. Bright, S. J. van der Walt, M. Brett, J. Wilson, K. J. Millman, N. Mayorov, A. R. J. Nelson, E. Jones, R. Kern, E. Larson, C. J. Carey, Í. Polat, Y. Feng, E. W. Moore, J. VanderPlas, D. Laxalde, J. Perktold, R. Cimrman, I. Henriksen, E. A. Quintero, C. R. Harris, A. M. Archibald, A. H. Ribeiro, F. Pedregosa, P. van Mulbregt and SciPy 1.0 Contributors, *Nat. Methods*, 2020, **17**, 261–272.

